Available online at www.sciencedirect.com
ScienceDirect
International Journal of Pharmaceutics 342 (2007) 176–183
INTERNATIONAL JOURNAL OF PHARMACEUTICS
www.elsevier.com/locate/ijpharm

Pore size distribution in tablets measured with a morphological sieve

Yu San Wu [a,*], Lucas J. van Vliet [b], Henderik W. Frijlink [a], Kees van der Voort Maarschalk [a,c]

[a] *Department of Pharmaceutical Technology and Biopharmacy, University of Groningen, Ant. Deusinglaan 1, 9713 AV Groningen, The Netherlands*
[b] *Quantitative Imaging Group, Department of Imaging Science & Technology, Faculty of Applied Sciences, Delft University of Technology, Delft, The Netherlands*
[c] *Department of Pharmaceutics, NV Organon, Oss, The Netherlands*

Received 14 December 2006; accepted 8 May 2007
Available online 16 May 2007

Abstract

Porosity and pore structure are important characteristics of tablets, since they influence mechanical strength and many other properties. This paper proposes an alternative method for the characterization of pore structure based on image analysis of SEM micrographs. SEM images were made of sodium chloride tablets made with three different particle sizes. The pore size distribution in these images was determined with a technique referred to as a morphological sieve. The results were compared to the pore size distributions as obtained with mercury porosimetry. The SEM images display small cracks inside the grains and small 'floating' grains inside the pore space. As these artifacts are induced in sample preparation, they need to be identified and removed from the images before analysis. The influence of the size of the discarded structures on the total porosity and the pore size distribution was investigated. The small 'floating' grains prevented the determination of the size of large pores, but had a negligible effect on the porosity. The removal of small cracks inside the grains had no effect on the pore size distribution but a large effect on the porosity. Based on the comparison of these results with the experimentally determined porosity, a maximum size for the structures that were to be removed was determined. The resulting pore size distributions were in the same order of magnitude as the results obtained with mercury porosimetry. Both methods display a comparable relative shift of the pore size distributions to larger sizes for tablets with increasing particle size. Therefore, it can be concluded this image analysis technique is a good method for the characterization of pore structure.

Keywords: Image analysis; Pore size distribution; Tabletting; Imaging; Porosity

1. Introduction

Porosity and pore structure are important characteristics of tablets since they influence relevant properties such as mechanical strength or the intrusion of water. Ryshkewitch and Duckworth established the relationship between bulk porosity and tensile strength, stating that there is an exponential relation between these two parameters (Duckworth, 1953; Ryshkewitch, 1953). More recently, it has also been shown that pore size influences tensile strength. For tablets of lactose and of lactose granules it was found that larger pores correlated with a lower tablet strength (Riepma et al., 1993; Zuurman et al., 1994; Juppo, 1995) and a similar relation was found for tablets of mannitol (Juppo, 1995; Westermarck et al., 1998) and glucose (Juppo, 1995).

Several techniques can be used to characterize pore structure. One of these techniques is gas permeametry which has been used to measure the tablet surface area and the mean pore radius of tablets (Ganderton and Selkirk, 1970; Alderborn et al., 1985; Wikberg and Alderborn, 1990). Another well-known technique is mercury porosimetry. This technique is commonly used to measure pore size distributions in pharmaceutical tablets since a wide range of pore diameters can be assessed.

Both methods suffer from disadvantages. For instance, with permeametry only a mean pore diameter or a surface area can be measured and the method is only suitable when the porosity is high. With mercury intrusion it is possible to obtain a pore size distribution assuming that the pore space is composed of tubular structures with a cylindrical shape. However, in real tablets this assumption is violated since the pores of a tablet will have irregular shapes. This effect causes a bias in the pore size distributions as obtained with mercury porosimetry. With mercury porosimetry it is also not possible to find out what the real shape of the pores is. Another disadvantage is that if pores are

* Corresponding author. Tel.: +31 50 3633282; fax: +31 50 3632500.
E-mail address: y.s.wu@rug.nl (Y.S. Wu).

0378-5173/$ – see front matter © 2007 Elsevier B.V. All rights reserved.
doi:10.1016/j.ijpharm.2007.05.011

not connected to the outside of the tablet, it will be impossible to measure pore size with this technique, since mercury is not able to enter the pores. With mercury porosimetry it is also not possible to determine the pore size at different locations in the tablet. Finally, mercury is preferably not used in many settings for environmental reasons.

With methods involving image analysis some of these disadvantages can be circumvented. For instance, by making images of different locations, it is possible to obtain results from different locations in the tablet. Mercury is not necessary and with image analysis it is possible to visualize the pore structure and to see how the pore size distribution was realized. Therefore, image analysis could be a valuable tool to assess pore structure.

A possible technique to analyze the pore structure in images is the morphological sieve. The morphological sieving method was first proposed by Matheron (1975). This image-processing tool can be used for the analysis of size distributions, but has a lot of other applications. An overview of these applications was given by Soille (1999). In the present paper we applied a morphological sieve to analyze the pore structure in tablets produced using particles of different sizes. Tablets were also analyzed with mercury intrusion porosimetry in order to compare the obtained pore size distributions.

2. Theoretical background

2.1. Morphological sieve

A granulometry is a size distribution obtained with image analysis using a morphological sieve (Luengo Hendriks et al., 2007). This way of sieving shows strong similarities to sieving a powder with a set of standard laboratory sieves. When using laboratory sieves, powder passes through sieves with increasing mesh sizes until the particles are too large to fall through. By measuring the amount of powder that stays behind on each sieve, a particle size distribution can be obtained.

A morphological sieve applies a similar principle in reverse order. Instead of real powder and laboratory sieves, a morphological sieve is applied to image structures using morphological filters. With these filters, structures smaller than the structuring element used are removed from the image (this is a discrepancy with the use of laboratory sieves where the large particles are removed first). By increasing the size of the structuring element, structures of increasing size are removed from the image. For each size of the structuring element, the number of pixels that is removed from the image is calculated. In this way a size distribution can be obtained.

A common way of applying a morphological sieve to an image is performing a morphological closing or opening operation with structuring elements of increasing size. These operations are complementary to each other. So if an opening is used to determine the size distribution for one phase out of an image consisting of two phases, a closing is used to determine the size distribution of the other phase.

The principle of removing structures from an image by using a closing operation on the pore space is illustrated in Fig. 1. In this figure, the black squares represent pixels of the grains, while the white area is part of the pore phase. A closing operation consists of a dilation followed by an erosion. The dilation with the structuring element is executed by placing the central pixel of the structuring element in every pixel of the grain and adding the neighboring pixels of the structuring element to this grain. After the dilation, the erosion is performed on the dilated figure. This is done by placing the central pixel of the structuring element in each of the pixels of the dilated figure and keeping this pixel if the entire structuring element is embedded in the grain of the intermediate figure. As can be seen in Fig. 1 this results is a complete disappearance of the small pore, while the closing operation only takes some corner pixels out of the large pore. By increasing the size of the structuring element, more and more pore space will be removed until all the pores are closed.

Looking at Fig. 1, it is easy to see that the structuring element has already filled the smaller pore. For the larger pore, the first size of the structuring element only rounds of the corners. However, a larger structuring element will make the pore space disappear completely as if the pore has been filled. A color coded example in the results section illustrates this principle.

By using the closing operation with structuring elements of increasing size, a relative cumulative size distribution can be obtained. A simplified form of the mathematical definition of the cumulative distribution (Luengo Hendriks et al., 2007) can be written as follows:

$$A_{\text{rel.cum}}(\varphi_R) = \frac{N_{\text{pixels removed from pore space}}(\varphi_R)}{N_{\text{pixels\_pore}}(\varphi_{R=0})} \quad (1)$$

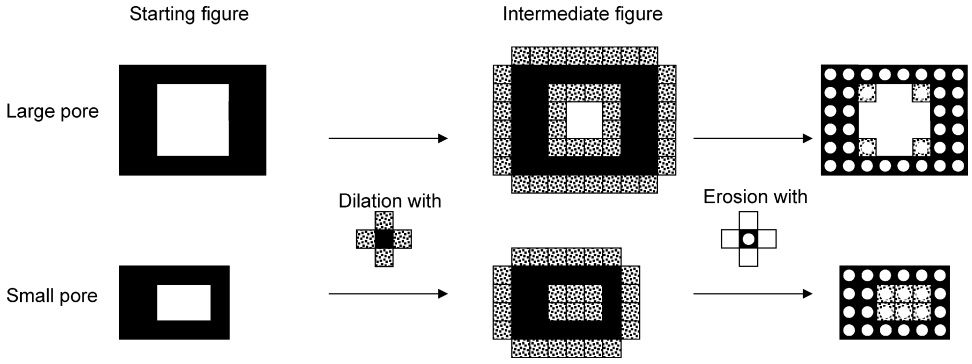

Fig. 1. Closing (dilation followed by an erosion) of the pores.

where $A_{\text{rel.cum}}(\varphi_R)$ is the area fraction removed from the pores as function of a closing with a structuring element with size R; $N_{\text{pixels removed from pore space}}(\varphi_R)$ the number of pixels removed from the pore space after closing with a structuring element with size R; $N_{\text{pixels\_pore}}(\varphi_{R=0})$ is the number of pixels in the pore phase after closing with a structuring element with size $R=0$ (i.e. number of pixels in the pores in the original image).

3. Experimental

3.1. Materials

The particle size fractions 75–106, 106–150 and 212–250 μm of sodium chloride (Chemically pure quality, Akzo Nobel, Hengelo, The Netherlands) were used for the tablet production. This fraction was obtained by 30 min vibratory sieving (Fritsch analysette 3, Germany) and 12 min air jet sieving (Alpine A200, Augsburg, Germany) over a sieve of 75, 106 or 212 μm to remove the fines. The true density of the sodium chloride as determined with helium pycnometry (Quantachrome, Syosset, NY, USA) was 2175 kg/m^3.

3.2. Tablet compaction

Tablets consisting of 500 mg sodium chloride were made by uni-axial compression in a round die with a diameter of 13 mm. Prior to compression the die was lubricated with magnesium stearate using a brush. The maximum compression force was 10 kN generated with a hydraulic press (ESH compaction apparatus, Hydro Mooi, Appingedam, The Netherlands). The rate of compaction was 0.2 kN/s.

After 2 days, the dimensions of each compact were measured with an electronic micrometer (Mitutoyo, Tokyo, Japan) and the weight of the compacts was measured using an analytical balance (Mettler-Toledo, Greifensee, Switzerland). From these data and the real density of sodium chloride the true porosity of the compacts was calculated.

3.3. Mercury intrusion

The pore size distribution of the compacts was measured with mercury intrusion porosimetry (Micromeritics, Model Autopore 9220, Norcross, GA, USA). For the measurement of the pore size distribution three compacts were used. Low pressure measurements were performed from 0 to 0.2 MPa. High pressure measurements were performed from 0.2 to 212 MPa. The surface tension of mercury was assumed to be 480 mN/m and the contact angle of mercury with the sodium chloride was assumed to be 140°.

3.4. Scanning electron microscopy

Compacts were embedded in glycol methacrylate and then cut with a microtome (Reichert-Jung 2050, Vienna, Australia) to obtain a smooth surface at the bottom of the compact. Scanning electron microscopic (SEM) images of these surfaces were made using a JEOL scanning electron microscope (JEOL, type JSM-6301F, Japan). Details about sample preparation and imaging protocols can be found in earlier work (Wu et al., 2005). We collected nine images per surface of different areas according to a fixed pattern as depicted in Fig. 2.

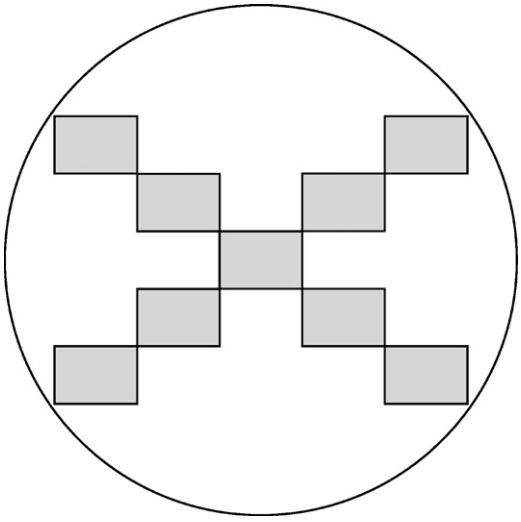

Fig. 2. Locations on the tablet surface of which images were taken.

3.5. Filtering of the image

The images used for the determination of the size distribution had a size of 2448 × 1681 pixels (1958 μm × 1344 μm), with a bimodal gray value [0,255] distribution representing the grains and the pores. The remaining images were subject to the following operations in Matlab (Version 7.0.4.356 R14, The Mathworks Inc.) and the DIPimage toolbox (Version 1.4.2, Quantitative Imaging Group, Delft University of Technology).

First, the gray scale image was clipped. This is a standard image-processing tool to remove extreme pixel values, narrowing the range of pixel values. The rationale of this operation is described in detail by Luengo Hendriks (Luengo Hendriks, 2004). In short, clipping is necessary because the computer algorithm decides whether pixels belong to either the pores or the grains on the basis of the gray values. If pixels in one grain have different gray values than pixels in another grain or if a grain or a pore has an uneven distribution of gray values, the size distribution becomes less accurate. Clipping the grayscale image compensates for that.

After clipping, small floating grains that were not connected to the rest of the matrix were removed from the image prior to the analysis. The size of the floating grains that were to be removed was varied in order to investigate the influence of the size of the removed grains on the total porosity and the pore size distribution in the images. Small cracks of varying sizes that were present inside the grains were also removed for the same purpose as for which the floating grains were removed. After these operations the total number of pixels in the pore phase was calculated. The porosity was then calculated as percentage of the pixels in the pore phase of the total number of pixels in the image.

3.6. Visualization

To visualize how the algorithm had generated the resulting size distribution, another algorithm was used that colors the pore space according to the size of the structuring element that removes area from the pores. This was done both before and after removal of floating grains and pores.

3.7. Calculation of the size distribution

The computer algorithm calculated the relative cumulative size distribution of the pores based on area. The measured 'projected' pore surface area was recalculated to a pore volume distribution with the assumption that the projection was the result of a spherical pore. (This method of calculation is similar to the commonly used calculation of particle sizes using the equivalent sphere diameter method based on projected surface area.) Out of this size distribution the size distribution based on volumes was calculated. For this calculation it was assumed that all pores were spherical, that the shape of the pores was not dependent on pore size, and that these spheres were cut through their center.

$$V_{\mathrm{rel},R_n} = \frac{(A_{\mathrm{rel.cum},R_n} - A_{\mathrm{rel.cum},R_{n-1}}) \times N_{\mathrm{pixels\_pore}} \times V_{\mathrm{sphere},R_n}}{A_{\mathrm{sphere},R_n}}$$

where V_{rel,R_n} is the relative volume fraction in the size class from R_{n-1} to R_n; R_n the size of the structuring element ($R_n > R_{n-1}$); $A_{\mathrm{rel.cum},R_n}$ the relative cumulative area fraction up to R_n; $N_{\mathrm{pixels\_pore}}$ the total number of pixels in the pore phase in an image; $V_{\mathrm{Sphere},R}$ the volume of a sphere with diameter R_n (in pixels); $A_{\mathrm{sphere},R}$ is the cross-sectional area of a sphere with diameter R_n after slicing through the center (in pixels).

Out of these results the relative cumulative volume distribution was calculated. The last step involved a conversion from pixels to micrometers. For this conversion it was derived from an original image with scale bar that 1 pixel had a size of $0.8\ \mu\mathrm{m} \times 0.8\ \mu\mathrm{m} = 0.64\ \mu\mathrm{m}^2$.

The relative shift of pore size distributions between the different particle sizes was calculated for both methods. This was done by calculating the pore diameter at 0.5 relative cumulative volume for each particle size and dividing this value by the pore diameter at 0.5 relative cumulative volume for the smallest particle size.

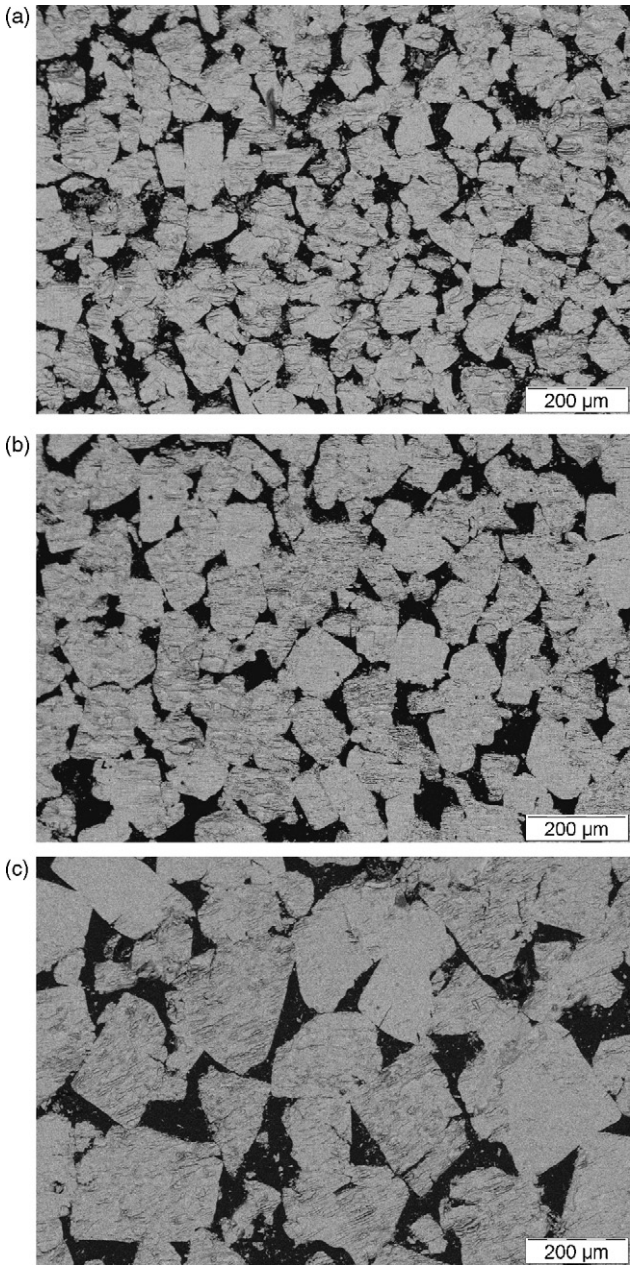

Fig. 3. (a) Part of an original SEM image of the surface of a tablet of 75–106 μm. (b) Part of an original SEM image of the surface of a tablet of 106–150 μm. (c) Part of an original SEM image of the surface of a tablet of 212–250 μm.

4. Results and discussion

4.1. Original image

Fig. 3 shows original SEM images of the surfaces of tablets made of the three different particle sizes. It can be seen that in some grains small cracks are present.

It can also be seen in the image that there are 'floating' grains in the pore phase. These grains are not connected to the rest of the grain matrix. In the original tablets it would have been impossible for these grains to float in the pore space and they probably stuck to larger grains. During embedding of the tablet the grains could float in the embedding medium and were fixated inside the pore space. 'Floating' grains will reduce the maximum pore size that will be found by the computer algorithm, since these grains function as a new starting point where the structuring element can start with the closing of the pore space. Thus, the floating grains will change the pore size distribution.

Because of the above-mentioned phenomena we considered it necessary to investigate the influence of the removal small pores and the removal of floating grains on the total porosity and the pore size distribution. This will be discussed in the following sections.

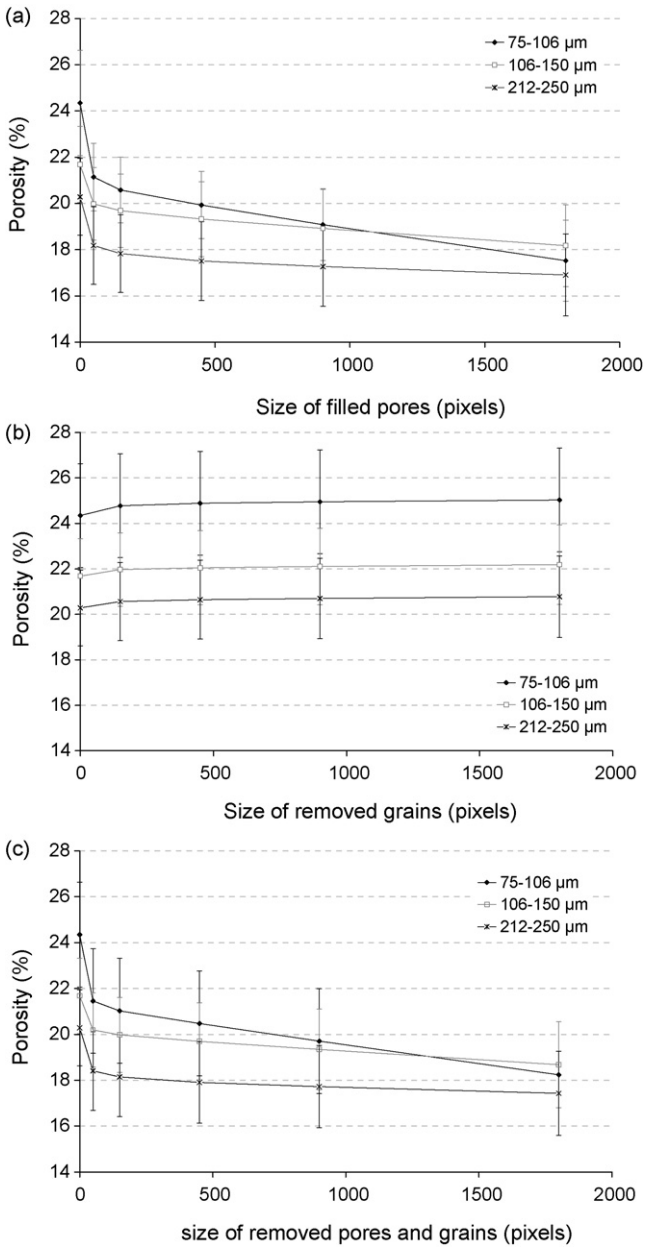

Fig. 4. (a) Porosity after filling of small pores. (b) Porosity after removal of small grains. (c) Porosity after removal of small pores and grains.

4.2. Influence of removal of floating grains and pores on the total porosity

Fig. 4 shows the influence of the filling of small pores and the removal of floating grains on the total porosity. It can be seen in Fig. 4a that with the removal of small pores the porosity decreases. This is logical since the removed pores are substituted with grain space. The filling of pores smaller than 50 pixels causes a tremendous decrease of the porosity. It should be noted that a pore of 50 pixels corresponds to an area of approximately $50 \times 0.64 = 32\ \mu m^2$.

Fig. 4b shows the effect of the removal of floating grains on the total porosity. It can be seen that the porosities increase with increasing size of the removed grains. However, the effect

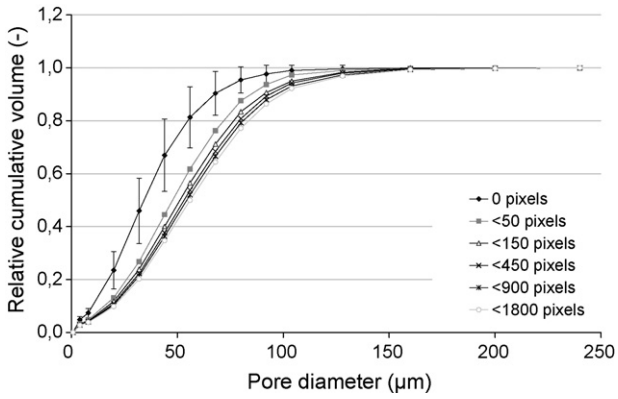

Fig. 5. Pore size distribution of tablet 212–250 μm before and after removal of small grains and pores of different sizes.

of the removal of the floating grains is insignificant, indicating that there are not many floating grains. There only seem to be floating grains smaller than 150 pixels, corresponding to grain sizes up to 96 μm^2.

Fig. 4c shows the relation between the porosity and the combined effect of removal of floating grains and pores. The results in this figure are obtained when the pores that are filled have the same size as the floating grains that have been removed. This figure actually shows the sum of the results in Fig. 4a and the results in Fig. 4b.

4.3. Influence of removal of small pores and floating grains on pore size distribution

The influence of the removal of small pores and grains on the pore size distribution was also investigated. It turned out that if only small cracks were removed, the size distribution did not change (data not shown). This was tested for cracks up to a size of 1800 pixels (1152 μm^2) and was found for all three particle sizes. It can be explained by the fact that small pores might be large in number, but do not have a large volume. Therefore, the removal of small cracks has a negligible effect on the volume distribution. However, the removal of floating grains did shift the pore size distribution to the right i.e. towards a larger pore diameter. This was also found when both pores and grains up to the same size were removed. Fig. 5 shows these results for the particle size 212–250 μm. It can be seen that removal of grains and pores smaller than 50 pixels has a pronounced effect, but that removal of pores and particles larger than 50 pixels has a negligible effect on the measured pore size distribution. The effect of removal of small pores and grains on the pore size distribution is similar for the other particle sizes (data not shown).

4.4. Choosing cracks and floating grains of what size need to be removed

It is known from stereology that the average area fraction of a phase, determined on sections through a volume, represents a good estimate of the volume fraction of this phase (Underwood, 1970). In our setting, this would mean that the area fraction of

the pores in the images would give a good estimate of the porosity in the tablet. However, the porosity measured in the images before removal of floating grains and pores is higher than the porosity measured by the volumetric method, which is a rather accurate method. This could indicate that the algorithm assigns too many pixels to the pore phase. As can be seen in Fig. 4a removing/filling only the small pores decreases the porosity significantly. In order to decide whether it is legitimate to remove these pores, one should ask where these small cracks originate from. Two possibilities are conceivable. The first one is that the small cracks are in fact artifacts induced by the use of the microtome. In that case, these cracks are not present in the physical situation and should be removed. The second possibility is that the cracks are enclosed in a grain, forming a vacuole inside a sodium chloride grain. These vacuoles are not accessible from the outside and are consequently also not accessible for helium gas during the helium pycnometery measurements. This implies that the vacuoles are already accounted for in the true density of the sodium chloride. These small cracks should thus be classified as grain space in the image analysis. For the removal of the floating grains, the discussion is slightly different. In the physical situation these grains are present, but it is impossible for them to 'float' in the pore space. The floating is caused by the embedding medium. So, as the small grains do not float in the physical situation and prevent the determination of large pore sizes, they should be removed before the determination of the pore size distribution.

From the above follows that before the pore size distribution is determined, it is necessary to fill the small cracks inside the grains (and not between the grains) and to remove small floating grains that are not connected to the grain matrix. The size of the grains to be removed and the size of the small cracks to be filled needs to be selected based on a physical model of the sample. For our system we have chosen to make the decision what sizes needed to be removed based on the resulting area fractions of the porosities in the images.

The porosities determined by the volumetric method were taken as the 'real' porosities, since this method is rather accurate. These porosities were compared to the results in Fig. 4c that were obtained by removing both small pores and floating grains. It turned out that to obtain the best resembling porosity different sizes had to be removed for the different particle sizes. For the particle size 75–106 μm pores and grains smaller than 450 pixels (288 μm^2) were removed, for the particle size 106–150 μm pores and particles smaller than 900 pixels (576 μm^2) were removed, and for the particle size 212–250 μm pores and particles with a size up to 1800 pixels (1152 μm^2) were removed. The removed structures were much smaller than the original grains. None of the removed cracks were connected to the pore matrix and none of the removed grains were connected to the grain matrix. The resulting porosities determined by the different methods are shown in Table 1.

Table 1
Average porosity (%) calculated with different methods

	75–106 μm	106–150 μm	212–250 μm
Volumetric	20.8 ($n=10$)	19.2 ($n=10$)	17.4 ($n=10$)
Morphological sieve (before filtering)	24.4 ($n=37$)	21.7 ($n=39$)	20.3 ($n=45$)
Morphological sieve (after filtering)	20.5 ($n=37$)	19.4 ($n=39$)	17.4 ($n=45$)
Mercury porosimetry	20.6 ($n=3$)	18.7 ($n=3$)	16.4 ($n=3$)

4.5. Color coded pore space

Fig. 6a shows the color coded pores in an image of a tablet surface of 212–250 μm before removal of the small cracks and grains. The color coding is shown below. It can be seen that small pores (purple color) are detected inside the grains and that small floating grains prevent the detection of large pores as was discussed in a previous section. Fig. 6b shows the color coded pores after the removal of small cracks and floating grains up to a size of 1800 pixels. This figure shows that after the removal small pores are not detected inside the grains anymore. It can also be seen that after removal of floating grains larger pores can be measured in the image. This clearly illustrates the importance of removal of the small grains and filling of the small cracks.

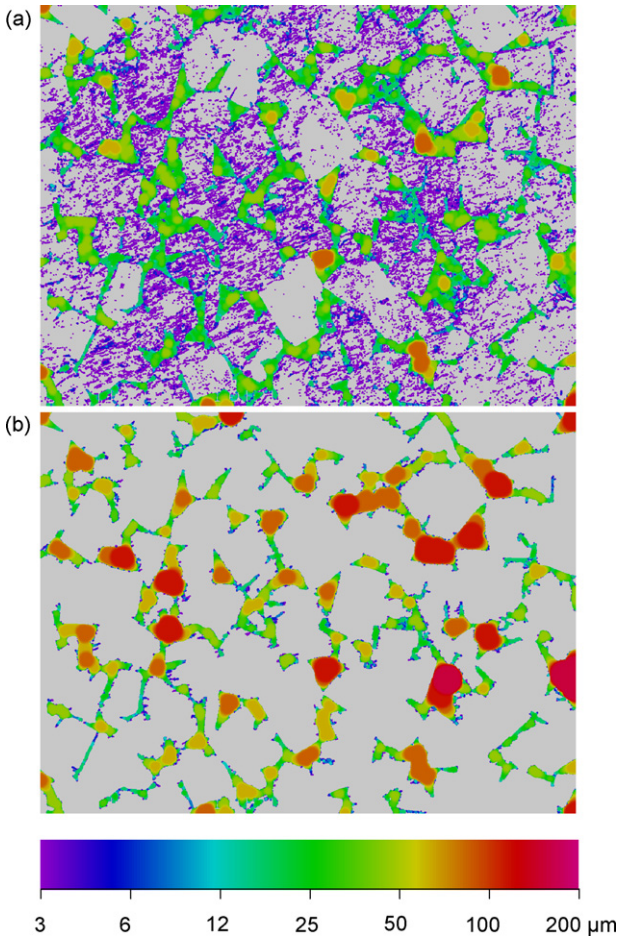

Fig. 6. (a) Color coded pore space before removal of small grains and pores. (b) Color coded pore space after removal of small grains and pores.

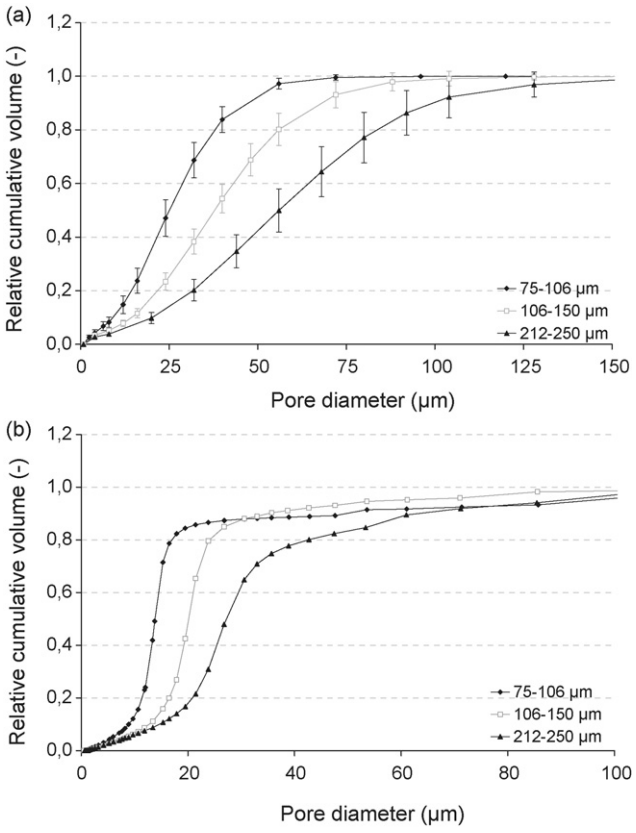

Fig. 7. (a) Cumulative size distribution measured with morphological sieve. (b) Cumulative size distribution measured with mercury porosimetry.

4.6. Size distribution for tablets of the different particle sizes

Fig. 7a shows the size distribution of the pores obtained with the morphological sieve after the removal of small cracks and floating grains of the appropriate sizes. It can be seen that there is a clear distinction between the pore size distributions in the tablets of the different particle sizes which shift towards larger pore diameters with increasing particle size. This can be confirmed by looking at the original SEM images in Fig. 3, where it is clear that the pores increase in size with increasing particle size. Other authors reported similar relations. Freitag et al. found that the use of a larger particle size resulted in larger pores for magnesium carbonate tablets (Freitag et al., 2004). An increase in pore size with increasing particle size has also been reported for lactose granules (Riepma et al., 1993) and sodium chloride tablets (Adolfsson et al., 1999). When larger particles are packed, the voids between them are usually larger than when smaller equally shaped particles are used.

4.7. Comparison with mercury porosimetry results

Fig. 7b shows the size distribution of the pores obtained by mercury porosimetry. These results also show that the pore sizes increase with increasing particle size. The shapes of the curves obtained by the two techniques are different. That the results of these two methods not exactly coincide, is comparable to a particle size analysis. With a particle size analysis the resulting size distribution is strongly dependent on the used method, and there is no method that gives the 'real' particle size distribution. Which method is most suitable depends on the situation. For the pore size analysis it is no different.

Table 2
Mean relative shift of pore size distribution expressed as the ratio of the pore diameter at 0.5 relative cumulative pore volume of each particle size and the pore diameter at 0.5 relative cumulative pore volume of the smallest particle size

	75–106 μm	106–150 μm	212–250 μm
Mercury porosimetry	1.00 ($n=3$)	1.46 ($n=3$)	1.97 ($n=3$)
Morphological sieve	1.00 ($n=37$)	1.51 ($n=39$)	2.23 ($n=45$)

In the case of the pore size distribution analyzed with both the image analysis and the mercury porosimetry, the dissimilarity in shape of the curves obtained with the two methods are caused by the different assumptions regarding the shape of the pores. With mercury porosimetry the pores are assumed to have a cylindrical shape. This shape is used to calculate the pore diameters from the pressures that are applied. A different shape will cause a different mapping of the pressures to pore diameters. For the morphological sieve method a spherical pore shape was assumed for the conversion from the area distribution to the volume distribution. For this conversion it was also assumed that all the spheres were cut through the center of the sphere, creating the largest circular cross-section possible. However, a randomly selected cross-section through a sphere of radius R yields a circle of radius r, with r in the interval 0 to R. A pore space composed of spheres of equal radius R, yields a measured distribution that is smeared out over a wide range of observed circles. The average radius is $\pi/4R$. This means that pore size distribution found here is broader than the real pore size distribution and that the real distribution has slightly larger pores.

So both methods rely on assumptions on the geometry and shape of the pore space that are incorrect as can be seen in the SEM images (Fig. 3). However, the results of both methods are in the same size range and both methods can differentiate between the pore sizes in the tablet of the different particle sizes. The relative shift of pore size distributions for the different particle sizes (Table 2) display an excellent correspondence between the two methods.

5. Conclusion

We conclude that the technique of measuring pore sizes in images of a tablet by the application of a morphological sieve is able to determine the pore size distribution of sodium chloride tablets. This method was even able to detect an increase in pore size when the tablets were produced of a larger particle size. The obtained values are similar to those obtained with mercury intrusion. Minor differences in both methods can be explained by the differences in the assumptions that are made on the geometry and shape of the pore space, which are different for the two techniques.

The method using the morphological sieve has the advantage that no mercury is needed and that it is applicable to all sorts of digital images (of tablet structures), making it possible to apply this technique on a wider scale. When doing so, one should be careful in selecting the right parameters for the preselection step based on a physical parameter of the sample. We used the measured porosity to select the size of the floating grains to be removed and the size of scratches to be filled. When the preselection step is properly done, this technique is an excellent method for the characterization of pore structure.

Acknowledgements

The authors wish to thank Mr. K. Zuurman for his help with the mercury porosimetry measurements and Mr. I. Stokroos for his help with the SEM during this study.

References

Adolfsson, A., Gustafsson, C., Nyström, C., 1999. Use of tablet tensile strength adjusted for surface area and mean interparticulate distance to evaluate dominating bonding mechanisms. Drug Dev. Ind. Pharm. 25, 753–764.

Alderborn, G., Duberg, M., Nyström, C., 1985. Studies on direct compression of tablets. X. Measurement of tablet surface area by permeametry. Powder Technol. 41, 49–56.

Duckworth, W.H., 1953. Discussion of Ryshkewitch paper by Winston Duckworth. J. Am. Ceram. Soc. 36, 68.

Freitag, F., Reincke, K., Runge, J., Grellman, W., Kleinebudde, P., 2004. How do roll compaction/dry granulation affect the tableting behaviour of inorganic materials? Microhardness of ribbons and mercury porosimetry measurements of tablets. Eur. J. Pharm. Sci. 22, 325–333.

Ganderton, D., Selkirk, A.B., 1970. The effect of granule properties on the pore structure of tablets of sucrose and lactose. J. Pharm. Pharmacol. 22, 345–353.

Juppo, A.M., 1995. Relationship between breaking force and pore structure of lactose, glucose and mannitol tablets. Int. J. Pharm. 127, 95–102.

Luengo Hendriks, C.L., van Kempen, G.M.P., van Vliet, L.J., 2007. Improving the accuracy of isotropic granulometries. Pattern Recogn. Lett. 28, 865–872.

Luengo Hendriks, C.L., 2004. Structure characterization using mathematical morphology. Ph.D. Thesis. Delft Technical University, The Netherlands, p. 115.

Matheron, G., 1975. Random Sets and Integral Geometry. Wiley, New York.

Riepma, K.A., Vromans, H., Zuurman, K., Lerk, C.F., 1993. The effect of dry granulation on the consolidation and compaction of crystalline lactose. Int. J. Pharm. 97, 29–38.

Ryshkewitch, E., 1953. Compression strength of porous sintered alumina and zirconia. J. Am. Ceram. Soc. 36, 65–68.

Soille, P., 1999. Morphological Image Analysis. Springer, Berlin.

Underwood, E.E., 1970. Quantitative Stereology. Addison-Wesley Publishing Company, Reading, MA, pp. 25–27.

Westermarck, S., Juppo, A.M., Kervinen, L., Yliruusi, J., 1998. Pore structure and surface area of mannitol powder, granules and tablets determined with mercury porosimetry and nitrogen adsorption. Eur. J. Pharm. Biopharm. 46, 61–68.

Wikberg, M., Alderborn, G., 1990. Compression characteristics of granulated materials. II. Evaluation of granule fragmenation during compression by tablet permeability and porosity measurements. Int. J. Pharm. 62, 229–241.

Wu, Y.S., Frijlink, H.W., van Vliet, L.J., Stokroos, I., van der Voort Maarschalk, K., 2005. Location dependent analysis of porosity and pore direction in tablets. Pharm. Res. 8, 1399–1405.

Zuurman, K., Riepma, K.A., Bolhuis, G.K., Vromans, H., Lerk, C.F., 1994. The relationship between bulk density and compactibility of lactose granulations. Int. J. Pharm. 102, 1–9.